Islamic Azad University

Journal of

Optoelectronical Nanostructures

Spring 2023 / Vol. 8, No. 2

Research Paper

Non-radiative Auger Current in a InGaN/GaN Multiple Quantum Well Laser Diode under Hydrostatic Pressure and Temperature

Rajab Yahyazadeh[*1], Zahra Hashempour[1]

[1]Department of Physics, Khoy Branch, Islamic Azad University, Khoy, Iran

Received: 24 Apr. 2023
Revised: 27 May. 2023
Accepted: 05 Jun. 2023
Published: 10 Jun. 2023

Use your device to scan and read the article online

Keywords:
Auger current, Overlap integrals, Laser diodes, Multi-quantum well.

Abstract:
This study employs a numerical model to analyze the non-radiative Auger current in c-plane InGaN/GaN multiple-quantum-well laser diodes (MQWLD) under hydrostatic pressure and temperature. Finite difference methods (FDMs) were used to acquire energy eigenvalues and their corresponding eigenfunctions of InGaN/GaN MQWLD. In addition, the hole eigenstates were calculated via a 6×6 **k.p** method under applied hydrostatic pressure and temperature. The calculations demonstrated that the hole-hole-electron (CHHS) and electron-electron-hole (CCCH) Auger coefficients had the largest contribution to the total Auger current (76% and 20%, respectively). Increasing the hydrostatic pressure could increase the amount of the carrier density and the electric field. On the other hand, this increase reduced the overlap integral of wave functions and the localized length of electrons, heavy, light and split of band holes. Also, for the hydrostatic pressure of about 10 GPa and the temperature of 300 K, the non-radiative Auger current has an optimum value of 334 A/cm^2. The results reveal that the elevated hydrostatic pressure and temperature play a positive and negative role in the performance of laser diodes.

Citation: Rajab Yahyazadeh, Zahra Hashempour. Non-radiative Auger current in a InGaN/GaN multiple quantum well laser diode under hydrostatic pressure and temperature. **Journal of Optoelectronical Nanostructures.** 2023; 8 (2): 81-107.

DOI: 10.30495/JOPN.2023.31803.1289

***Corresponding author:** Rajab Yahyazadeh
Address: Department of Physics, Khoy Branch, Islamic Azad University, Khoy, Iran
Tell: 00989143451741 **Email:** rajab.yahyazadeh@iaukhoy.ac.ir

1. INTRODUCTION

Non-radiative recombination is performed in the form of deep and shallow traps, interface roughness, and defects, as well as band-to-band and phonon-assisted Auger recombination (BBAR & PAAR) [1-5]. The Auger recombination is one of the important mechanisms in reducing the efficiency of photovoltaic devices [6-9]. BBAR is one of the essential non-radiative recombination techniques that has attracted the attention of different researchers in the field of InGaN/GaN photovoltaic devices [10-12]. Auger recombination is the most important parameter to obtain Auger coefficient and Auger current. Various numerical and analytical models have been used to calculate the Auger and lifetime recombination. Picozzi et al. studied the lifetime of this Auger through the first-principle detail balance based on the density function method at different carrier concentrations in semiconductors [13]. Likewise, Anatoli et al. evaluated the effect of temperature and well width on the Auger recombination using the Khans model in a semiconductor quantum well [14]. In addition, Piperk et al. investigated the dependence of the Auger coefficient on the carrier density, band gap, and wavelength through the ABC model on gallium nitride (GaN)- and nitride-based photovoltaic devices [7, 15]. McMahan et al. also focused on the atomistic analysis of Auger recombination in InGaN/GaN quantum wells under temperature [16]. Non-radiative Auger recombination generates a non-radiative current in photovoltaic devices such as solar cells, lasers, and diodes. Therefore, it is necessary to carefully study the dependence of all parameters to be effective in this recombination under external perturbations such as hydrostatic pressure or temperature. In this regard, the most important parameters are carrier density, effective band gap energy, carrier energy, built-in polarization field, and carrier localization length and overlap integral of wave functions. In this paper, changes in all the above-mentioned parameters are calculated and investigated under hydrostatic pressure and temperature in InGaN/GaN multiple-quantum well laser diodes. The Auger recombination rate is one of the most essential parameters in calculating Auger coefficient and the Auger current of laser diodes. Thus, the careful study of Auger current requires precise investigation of the Auger recombination rate, which is the main purpose of this paper under hydrostatic pressure and temperature. The use of five vital parameters, including effective mass, energy gap, lattice constants, dielectric constant and quantum barrier, and well thickness, is the most significant advantage of this numerical method and the innovation of this work., including; all the mentioned parameters simultaneously depend on hydrostatic pressure and temperature. This

study has also addressed the effect of hydrostatic pressure and temperature on the energy of heavy, light, and split-off band holes. In this model, the conduction band energy, wave functions, Fermi level, and energy subbands are obtained from the self-consistent solution of Schrödinger and Poisson equations. The current study also considered the effective width of the quantum wells, which depends on the carrier density, which is not constant. It should be noted that the Femi level has also been computed using another method that enables convergence in a sophisticated way [17]. The hole valence band (heavy, light, and split-off band holes) energy, wave functions, and energy subbands are calculated using a k.p method.

2. CALCULATION MODEL

The quantum-well laser diodes(QWLD) consists of a multiple-quantum-well structure in the intrinsic region of a p–i–n. The MQW structure introduced for the model is constructed by a $In_mGa_{1-m}N$ with lower indium molar fraction (m=0.3) for barriers and m=0.4 for wells (Fig. 1). The sample used in modeling is the p–i–n laser diodes with an InGaN/GaN MQWLD structure within the i-region. The p and n regions are based on GaN. The donor and acceptor concentrations in the n- and p-region materials are assumed to be the same as $0.1\times10^{18}cm^{-3}$, and 10 wells are considered in the current work. In addition, atmospheric and hydrostatic pressures are taken into account (i.e., at zero hydrostatic pressure), but only atmospheric pressure is applied for evaluation. Both Schrödinger and Poisson equations must be solved to obtain accurate values for Fermi energy, the energies of quantized levels within the two-dimensional electron gas (2DEG), potential profiles, wave function, and the sheet carrier concentration for 2DEG in InGaN/GaN heterostructures. This is achieved by solving Schrödinger's equation and simultaneously taking into account the electrostatic potential obtained from Poisson's equation, as well as the image and exchange-correlation potentials using the three-point finite difference method (see Appendix A) [18]. In the Schrödinger equation, built-in potential energy is considered, which is the potential energy induced by spontaneous (SP) and piezoelectric (PZ) polarization charges [19-21]. In this work, five parameters are used, including effective mass, energy gap, lattice constants, dielectric constant and quantum barrier, and well thickness, which simultaneously rely on hydrostatic pressure and temperature [22-24]. In our strained InGaN/GaN quantum wells, the conduction bands are assumed to be parabolic, and nonparabolic valence bands are computed by a 6 x 6 **k.p** method [25-28]. To calculate the BBAR rate in InGaN/GaN MQWs, we broadly follow

the presented method in previous research [29, 30]. We will only focus on the CHHS (one electron ($1'$) and two heavy holes ($1,2$) and one split of band hole ($2'$)) Auger process because CHHL (one electron, two heavy holes, and light hole) and CCCH (three electrons and one heavy hole) processes can be derived by a similar way. Auger processes involving phonons are generally not important for relative consideration at room temperature; here as a result, only three BBARs are considered in this study [29]. From Fermis's Golden Rule, the Auger transition rate per unit volume for the CHHS process is given by [30]:

$$R_w = \frac{1}{4\pi\hbar L_{eff}}\left(\frac{e^2}{4\pi\varepsilon_w}\right)^2\left(\frac{4\pi}{(2\pi)^3}\right)^2 \times \sum_{allE_z}\int\int\int\int \overbrace{|\boldsymbol{k}\text{-}\boldsymbol{k}'|^{-2}A_k^2}^{M}\delta(\boldsymbol{k_1}\text{-}\boldsymbol{k_{1'}}+\boldsymbol{k_2}\text{-}\boldsymbol{k_{2'}})P_{1,1',2,2'}\delta(E)d^2\boldsymbol{k}_1 d^2\boldsymbol{k}_{1'} d^2\boldsymbol{k}_2 d^2\boldsymbol{k}_{2'} \quad (1)$$

where $L_{eff} = (1/n)\int_0^{L_{InGaN}} zn(z)dz$ represents the effective width of the 2DEG channel [31]. Further, $n(z)$ and ε_w denote quantum well sheet density along the growth direction (z-direction) and the dielectric constant of the InGaN, respectively. Furthermore, $\delta(E)$ expresses energy conservation between initial (particles $1,2$) and final ($1',2'$) states, M is the matix element of Coulomb interaction potential between two holes, and A_k is the overlap integral. Moreover, $P_{1,1',2,2'} \approx f_{v1}f_{c1'}f_{v2}[1-f_{v2'}]$ account for sate occupations. The approximation is employed considering that the excited carrier has extremely high energy. Additionally, $f_c = 1/(1+\exp(E_c - E_{f_c})/k_bT)$ and $f_v = 1/(1+\exp[(E_v - E_{fv})/k_bT])$ are the Fermi-Dirac distribution for the electrons of conduction bands and holes in valence bands, respectively, where E_c and E_v are the quantized electron and hole energy levels, respectively. In addition, E_{f_c} and E_{f_v} represent the electron and hole quasi-Fermi levels, respectively. In relation 1, all the energies of the allowed transitions related to the subbands of the carriers are considered in the z-direction, following the selection rule. A detailed study of the effect of pressure on Auger recombination requires a detailed study of each of these parameters. The relation of the overlap integral in the Auger recombination is as follows [30]:

$$A_k = F_{11'}F_{22'}\iint dz_1 dz_2 \phi_1(z_1)\phi_{1'}(z_1)\phi_2(z_2)\phi_{2'}(z_2)e^{-|\mathbf{k_1}-\mathbf{k_{1'}}||z_1-z_2|} = I_{11'}(|\boldsymbol{k_1}-\boldsymbol{k_{1'}}|)I_{22'}(-|\boldsymbol{k_1}-\boldsymbol{k_{1'}}|) \quad (2)$$

where the particle state in the quantum well is represented by the product of a localized Bloch wave function, a plain wave term, and a confined-state wave function (ϕ). Further, k and $k_{1'}$ are the 2D wave vectors in the plain of the well carrier $\{1,1'\}$, respectively. At the beginning of each of the recombination stages (CHHS, CCCH, & CHHL), first, the electron and the hole must be recombined $(1,1')$ until the second stage $(2,2')$. In relation A_k, the integral contribution of the electron and hole overlap, $I_{eh} = I_{11'} = F_{11'}\int dz_1\phi_1(z_1)\phi_{1'}(z_1)e^{-|k_1-k_{1'}|.z_1}$, is the most important parameter to start the recombination. Furthermore, $I_{11'}$ denotes the overlap integral between the localized (the subband state in quantum wells) states. Moreover, $I_{22'}(-|\boldsymbol{k}-\boldsymbol{k'}|) = I_{hx} = F_{22'}\int dz_2\phi_2(z_2)\phi_{2'}(z_2)e^{-|\mathbf{k_1}-\mathbf{k_{1'}}|.z_2}$ indicates the overlap integral between the localized and excited (electron or hole) states. The excited states of particle $2'$ may be bound (subband) or unbound (even or odd) [29]. In this case, the contribution of each of these bound and unbound states in the Auger recombination will be R_A^b, R_A^e, and R_A^o, respectively [30], where b, e, and o represent bound, even, and odd, respectively. The overlap function of the electron and hole is non-linear with respect to $|\boldsymbol{k_1}-\boldsymbol{k_{1'}}|$. Additionally, $F_{11'} = (\alpha_{CH}|\boldsymbol{k_1}-\boldsymbol{k_{1'}}|)/E_g$ and $F_{22'} = (\alpha_{SH}|\boldsymbol{k_1}-\boldsymbol{k_{1'}}|)/E_g$ are the overlap integral of localized Bloch function between carrier $\{1,1'\}$ and $\{2,2'\}$, respectively. $\alpha_{SH} = -(\hbar^2/4m_0)\{[(m_0/m_l)+(m_0/m_H)+(m_0/m_S)-3]\}$ and $\alpha_{CH} = (\hbar^2/4m_0)[(m/m_c)-1]$ are the overlap parameter.

To investigate external perturbation such as pressure and the effect of the overlap integral, which has a direct relationship with the quantum confinement, the wave functions of the first subband of the carriers (ψ) were considered to calculate the localization length in the z axis as $(\Delta z) = \int|(z-\langle z\rangle)\psi|^2 dz$, where $\langle z\rangle = \int z|\psi|^2 dz$ [32]. The limits of the integral are taken into account from the center of the neighboring barrier adjacent to the center of the quantum well.

The effective mass of the carriers in each of the subbands of the quantum wells (electrons and holes) can be calculated after determining the effective mass of the carriers in the GaN barrier and the InGaN/GaN well [33, 34]. Binary effective mass parameters are linearly interpolated to obtain InGaN values. The numerical values of the valence band effective mass parameters (Ai) and deformation potentials (Di) from reference 38 have been used in this study. The effective masses in $m^*_{In_xGa_{1-x}N}$ barriers can be obtained by determining the effective masses of carriers in quantum wells through the ternary formula $1/m^*_{In_xGa_{1-x}N}=[(1-x)/m^*_{InN}]+x/m^*_{GaN}$ [35-37].

The recombination relationship for the InGaN quantum barrier in the MQW region is the same as relation 1, with the difference that the $\sum_{allEz}$ is converted into an integral and L_{eff} is removed from the denominator, and $V(r)=(q^2/r\varepsilon_{InGaN})\exp(-\lambda r)$ is the coulomb integration potential in matrix element relation (M). Where $\lambda=(4\pi q^2[n_b+p_b]/\varepsilon_{InGaN}k_bT)^{1/2}$ is reciprocal screening lengths, $n_b(z)=2(2\pi m^*_{eb}k_bT/h^2)^{3/2}F_{1/2}(\eta_c)$ and $p_b(z)=2(2\pi m^*_h k_bT/h^2)^{3/2}F_{1/2}(\eta_v)$ are electron and hole densities in the respectively [30, 38]. $F_{1/2}(\eta)$, is the Fermi-Dirac integral of order $1/2$.

Finally, the effective Auger coefficient in quantum well and barrier is defined as:

$$C_{w,b}(InGaN)=\overbrace{[R_{w,b}(CHHS)/\bar{p}_{w,b}{}^2\bar{n}_{w,b}]}^{C_{w,b}(CHHS)}+\overbrace{[R_w(CHHL)/\bar{p}_{w,b}{}^2\bar{n}_{w,b}]}^{C_{w,b}(CHHL)}+\overbrace{[R_{w,b}(CCCH)/\bar{n}_{w,b}{}^2\bar{p}_{w,b}]}^{C_{w,b}(CCCH)} \quad (3)$$

where $\bar{n}_{w,b}$ and $\bar{p}_{w,b}$ are the average electron and hole density inside the quantum wells and barriers[39-43]. The average value is due to the dependence on the location of carriers and their non-uniformity inside the quantum wells. The 2D Auger recombination rate and coefficient can be translated into common 3D rates using the quantum well thickness, which are $R_w=R_{2D}/L_{eff}$ and $C_w=L^2_{eff}C_{2D}$ [10] . By determining the Auger coefficient and density of the carriers, the Auger current is obtained from the following equation [44,45].

$$J_{w,b} = N_{w,b} qL_{w,b} ([C_{w,b}(CHHS) + C_{w,b}(CHHL)] n_{w,b} p_{w,b}^2 + C_{w,b}(CCCH) n_{w,b}^2 p) \quad (4)$$

Finally, $J_A = J_w + J_b$ is the total Auger current in the multiple-quantum-well region. If $C_A(CHHS)$ is greater than all Auger coefficients, the Auger current is $J_{w,b} \approx N_{w,b} qL_{w,b} C_{w,b}(CHHS) n_{w,b} p_{w,b}^2$.

3. Results and Discussion

In this paper, a numerical model was presented to calculate the optical and electrical parameters of *InGaN / GaN* multiple-quantum-well laser diodes (MQWLD) and investigate the effect of hydrostatic pressure and temperature. In addition, Schrödinger's and Poisson's differential equations were solved by the finite difference method. However, the iterative method [18,46] was used in the step of the self-consistent solution of Schrödinger-Poisson equations. The convergence is obtained when the difference in the Fermi level is associated with two consecutive iterations ($E_{F(n)} - E_{F(n-1)}$) and is smaller than $10^{-4} eV$. The same grid mesh was employed during the calculations for both Poisson and Schrödinger equations. The hole eigenstates were computed using a 6×6 **k.p** method. Conduction and valence bands with the location of quantum wells (electrons and holes), valence bands for light, heavy, and split-off band holes are shown in Fig. 2. To evaluate parameters related to the LED and start Auger recombination, a positive voltage of 1.5 V was applied to region p-GaN. In this case, the multi-quantum wells of electrons and holes are below the Fermi level (Fig. 1).

The inset of Fig. 2 represents the variation of the interface polarization charge density (σ_b) as a function of the hydrostatic pressure and temperature. This phenomenon is related to the correction of the atomic distances of the crystal lattice by external pressure and temperature. As a result, the centers of positive (holes) and negative (electrons) charges diverge and converge, respectively, leading to a change in polarization. With the increase in hydrostatic pressure, the lattice constants increase. However, the temperature increase acts opposite to the pressure, thereby reducing the atomic distance and decreasing the polarization. Fig. 3 shows an example of a change in an electron quantum well (position -50 nm) to study the changes in the well. By increasing the hydrostatic pressure in the range of 0-10 Gpa, the quantum well depth increases to 24 meV. In addition, by increasing the temperature in the range of 300-600 K, quantum well depth decreases to 20 meV.

According to Figs. 3a and 3b, polarization changes cause a change in the internal and total electric fields. For the pressure from 0 to 10 GPa, the electric field increases in the multiple-quantum well by 0.77 MV/cm, and a temperature rise in the range of 300-600 K reduces this field to 0.57 MV/cm. Further, the hole quantum well in position 150 nm and the electron quantum well in position -50 nm are $6.1 MV/cm$ and $3.2 MV/cm$, respectively. An increase in the electric field and interface polarization charge density causes an increase in carrier density (Figs. 3c-3f). Moreover, by increasing pressure by 10 GPa, the density of holes and electrons increase, and carriers in quantum wells (position -50 and 150 nm) are injected into the region of multiple-quantum wells, affecting the Auger recombination. The average density increase in the region of the multiple-quantum-well is $0.56\times10^{19} cm^{-3}$ and $0.75\times10^{19} cm^{-3}$ for electrons and holes, respectively. But with increasing temperature in the range of 300-600, the average density of holes and electrons decreases to $0.45\times10^{19} cm^{-3}$ and $0.62\times10^{19} cm^{-3}$, respectively.

Effective masses play the most important role in determining Auger recombination. Also, it is necessary to know the dependence on external perturbation, such as hydrostatic pressure and temperature. For this purpose, it is necessary to calculate the band structure of valence carriers; this process for quantum well and barrier InGaN/GaN is shown in Figs. 4 and 5. According to Fig. 4, in the direction of the in-plane wave vector (kx or ky), all bands are non-parabolic energy. Heavy holes are independent of pressure and temperature, and the graph slope is almost constant with the change of pressure and temperature. These points suggest that the effective mass of heavy holes remains unchanged with the increase of the wave vector, temperature, and pressure. However, light and split-off holes and their effective masses (i.e., the radius of curvature) change with increasing pressure and temperature. Accordingly, the effective mass of light holes almost approaches heavy holes after the wave vector of 1.03 nm^{-1}. These mass changes with pressure and temperature, and wave vectors are effective in computing the threshold voltage. According to Fig. 4, a pressure increase of 10 Gpa (at the band edge k = 0) causes a change in the energy of 42, 48, and 290 meV for heavy, light, and split-off holes, respectively. Besides, an increase in the temperature in the range of 300-600 K causes a change in the energy of 31, 35, and 110 meV for heavy, light, and split-off holes, respectively. The effective mass of split-off holes is lower than that of light holes, and they tend to receive energy from electron-hole recombination in Auger recombination. Therefore, the non-radiative recombination of CHHS is expected to be higher than that of CHHL for the InGaN/GaN quantum well. Fig. 5 can be

explained similar to the quantum well. By specifying the band structures, the effective masses can be calculated.

The overlap integral can be determined after determining the effective masses of carriers. In the overlap integral A_k, there is an overlap of electron and hole I_{eh}, in all recombination processes. Here, the overlap of the wave functions (the first subband of electrons and heavy holes) versus the transfer momentum ($k_{11'} = k_1 - k_{1'}$) is checked at different pressures (Fig. 6). Based on the results, increasing the pressure reduces the overlap of electron and hole wave functions but increasing the temperature increases the overlap. According to Fig. 6, the overlap is a non-linear function depending on the size of the transfer momentum. In the small transfer momentum, the overlap and recombination are reduced so that the hydrostatic pressure and temperature will have a reduced role in the recombination. The effect of hydrostatic pressure and temperature on the transfer momentum near the origin (non-resonant) is small. In the resonance mode ($(k_{11'} = k_1 - k_{1'})$), the energy of the transition ($(\hbar^2 k_{11'}^2 / (2m_c) = E_{11'}^{e,hh})$) becomes the same as that between heavy and split-off holes in the direct transition. The overlap of wave functions is one of the most important parameters in Auger recombination. The overlap integral also depends on the overlap integral I_{hx} between the localized and excited (electron and hole) states. In this study, both overlap integrals were compared by plotting their overlap in the positive part of $k_{11'}$. Therefore, the overlap integral I_{hx} is normally smaller than I_{eh}. As shown, the contribution of 85% of the total overlap integral is related to I_{eh}, and it is under the pressure and temperature the most changes. To more precisely investigate the effect of pressure and temperature on the carrier overlap, we draw the first subband wave functions for the quantum well (at position 45-50 nm, Fig. 7) and then obtained the localization length (Fig. 8). According to Fig. 7, the wave functions of heavy holes are more localized than all carriers, while those of electrons and split-off holes are delocalized. By plotting the localization length based on Fig. 8, with increasing pressure by 10 GPa, the localization length of heavy holes and electrons decreases by 1 and 3.8 nm, respectively. The least impact of pressure is on heavy holes; thus, unlike electrons that are affected by pressure, heavy holes can participate more in the CHHS Auger process. As a result, by increasing pressure by 10 GPa, the depth of the quantum well, the quantum confinement of the carriers, and the localized length of all carriers are greater. But the localization length for increasing temperature (the inset of Fig. 2) is exactly the opposite of the explanation of the localization length at different pressures. This outcome is related to the decrease

in polarization and internal field with increasing temperature, explained in Figs. 2 and 3.

The contribution of each of the recombination rates is shown in Figs. 9 and 10. As can be seen, the highest rate is related to $R(CHHS)$ due to the localization length of heavy holes, which was explained earlier. To check the contribution of each Auger recombination, we separately draw the recombination coefficient (quantum well and barrier) of all three processes (Fig. 11). As illustrated, the contribution of CHHS is the highest. This issue is related to the small effect of pressure on the localization length of heavy holes. As shown in Fig. 11a, the share of CHHS, CCCH, and CHHL is 82, 15, and 3% in the quantum well Auger coefficient, respectively. CHHL has a lower effect than heavy holes due to the high density of heavy holes, which is not usually considered. According to Figs. 11a and 11c, increasing the hydrostatic pressure by 10 GPa decreases the effective Auger coefficient up to $2.1\times10^{-31}cm^6s^{-1}$ and $0.6\times10^{-31}cm^6s^{-1}$ in the multiple-quantum well and barrier regions, respectively. Also, increasing the temperature in the range of 300-600K increases these coefficients up to $1.2\times10^{-31}cm^6s^{-1}$ and $0.2\times10^{-31}cm^6s^{-1}$ in the multiple-quantum well and barrier regions, respectively (Figs. 11b and 11d).

The calculated Auger recombination rate values are used to compute the Auger coefficients. The computed performance Auger coefficients are then contrasted with the theoretical and experimental in the literature [9,15, 50 55-57] presented in Table 1. We can see that Auger coefficient in well and barrier are similar to those presented in earlier reports by Laubsch et al. and Kioupakis et al. The Auger current under different hydrostatic pressures and temperature can be determined after calculating the density of carriers and the Auger coefficient (Fig. 12). Increasing the pressure by 10 GPa decreases the total Auger current by 96 A/cm^2. Also, increasing the temperature in the range 300-600 increases the total Auger current by 73 A/cm^2. Overall, the performance of the laser diode is better when the non-radiative Auger current is lower. Thus, hydrostatic pressure plays a positive role in the performance of laser diodes. Furthermore, for the hydrostatic pressure of about 10 GPa and the temperature of 300 K, the non-radiative Auger current has an optimum value of 334 A/cm^2 (Fig. 13).

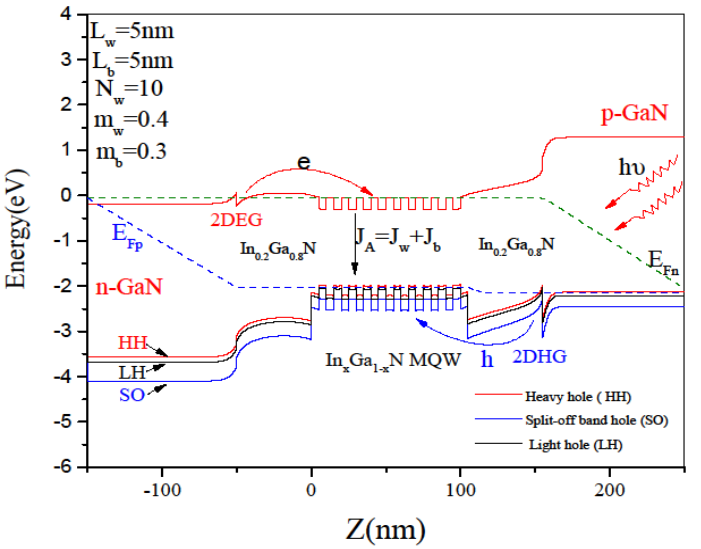

Fig. 1. The conduction (C.B) and valence (V.B) band energy of InGaN/GaN MQW laser diodes as a function of the distance under different hydrostatic pressure.

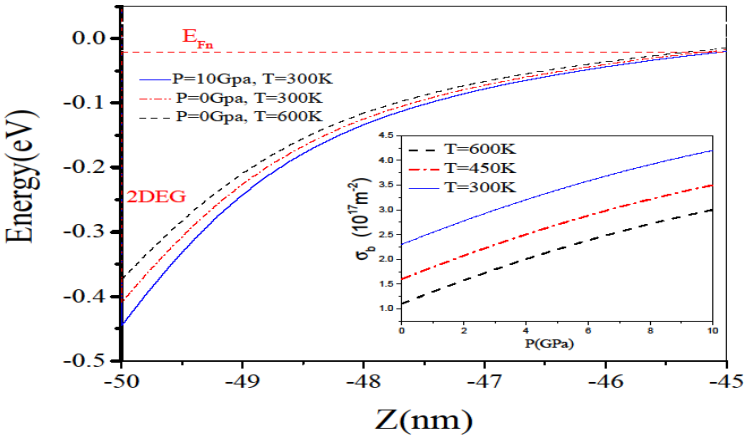

Fig. 2. The quantum-well conduction band energy as a function of the distance under different hydrostatic pressures temperature. The inset indicates the variation of InGaN/GaN interface polarization charge density σ_b as a function of the hydrostatic pressure and temperature.

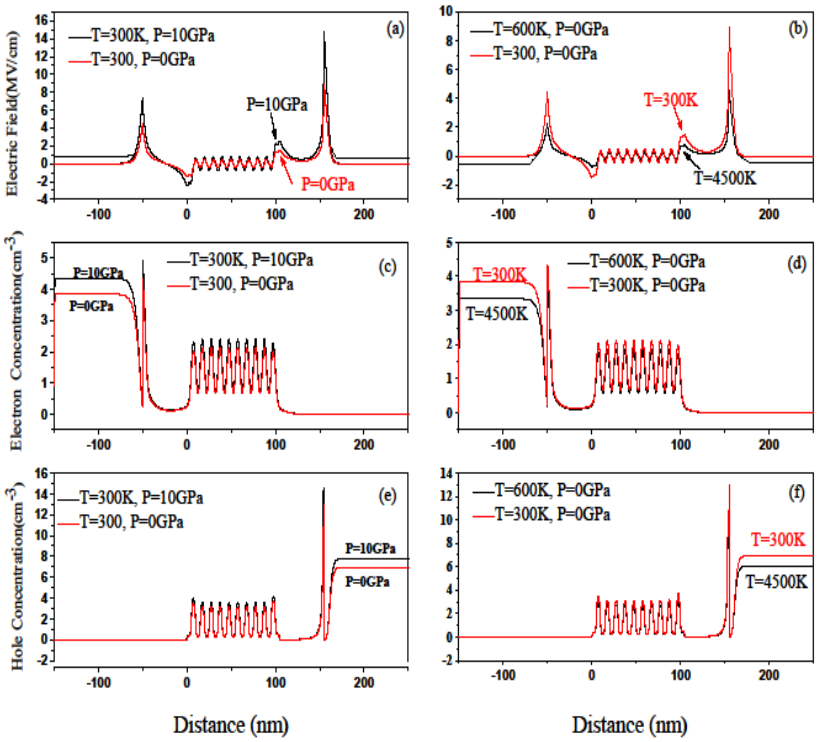

Fig. 3. Electric field (a, b), electron (c, d), and hole (e, f) concentration of InGaN/GaN MQW laser diodes as a function of the distance under different hydrostatic pressure and temperature.

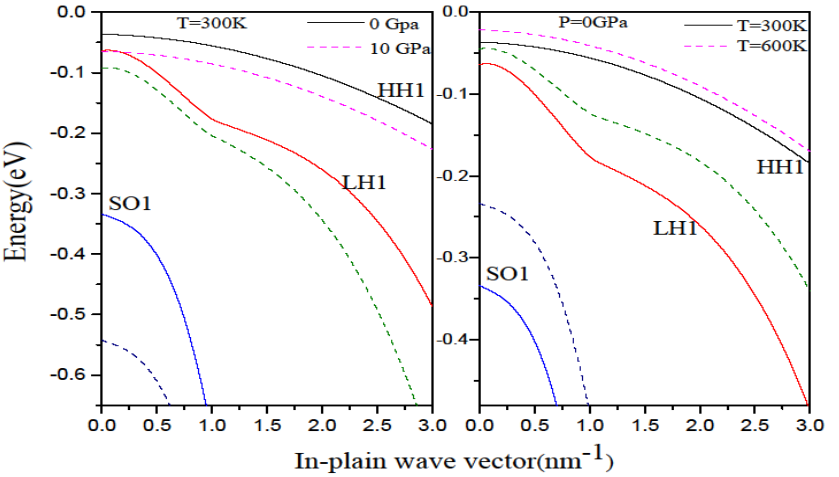

Fig. 4. The valence band structure of heavy-hole (HH), Light-hole (LH), and split-off hole (SO) band InGaN/GaN quantum well plotted along the k_x for hydrostatic pressure and temperature of 0 Gpa and 300K (solid lines) and 10 GPa and 600K (dashed lines), respectively.

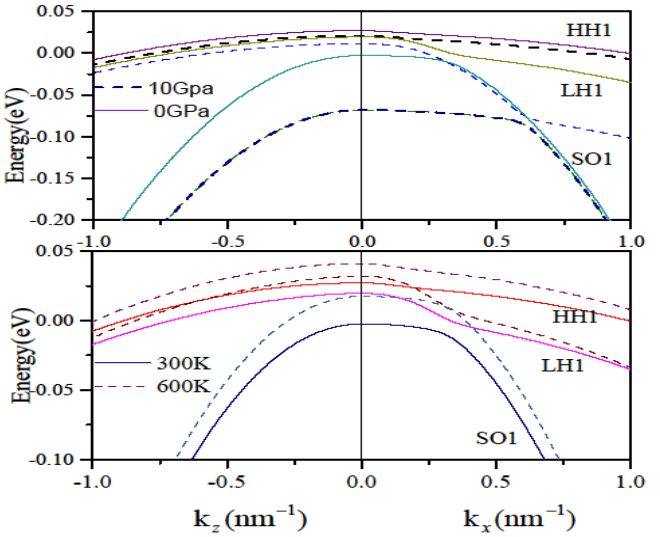

Fig. 5. The valence band structure of heavy-hole (HH), Light-hole (LH), and split-off hole (SO) band InGaN quantum barrier is plotted along the k_x and k_z for different hydrostatic pressure and temperature.

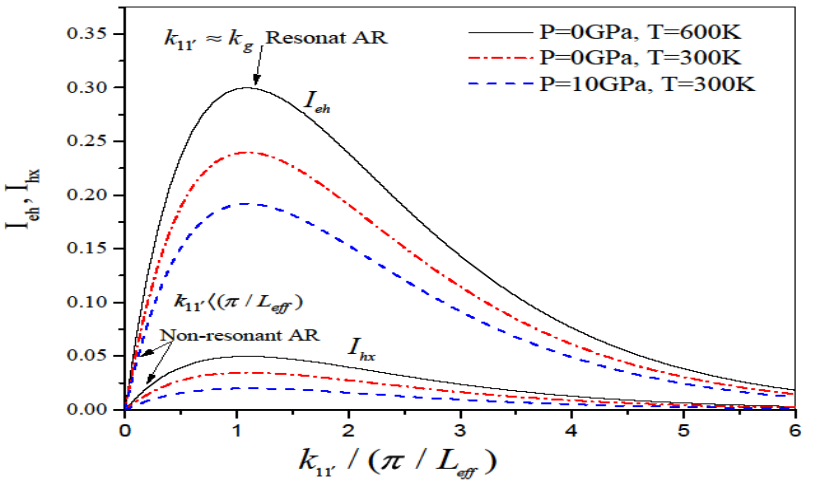

Fig. 6. Overlap integrals versus transferred momentum $k_{11'}$ for InGaN/GaN MQW laser diodes under different hydrostatic pressures.

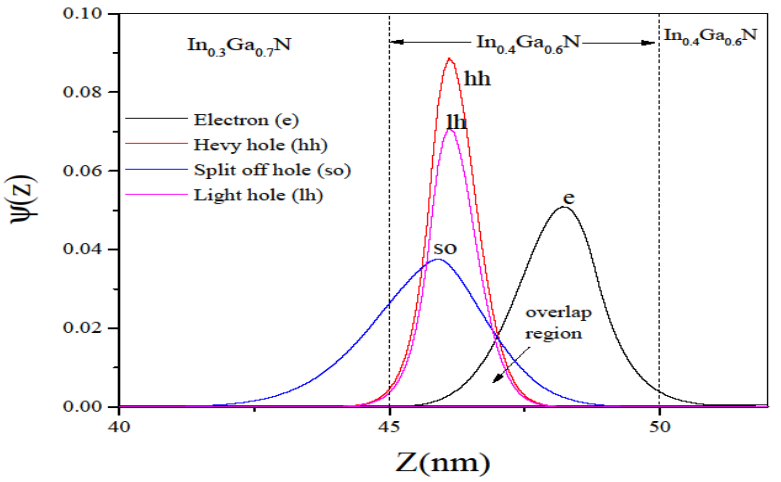

Fig. 7. The first subband electron wave function ψ(z) versus the distance for InGaN/GaN MQW laser diodes under different hydrostatic pressures for the heavy hole (hh), light hole (lh), electron (e), and split-off band hole (so) with the quantum well in positions 45 to 50 nm.

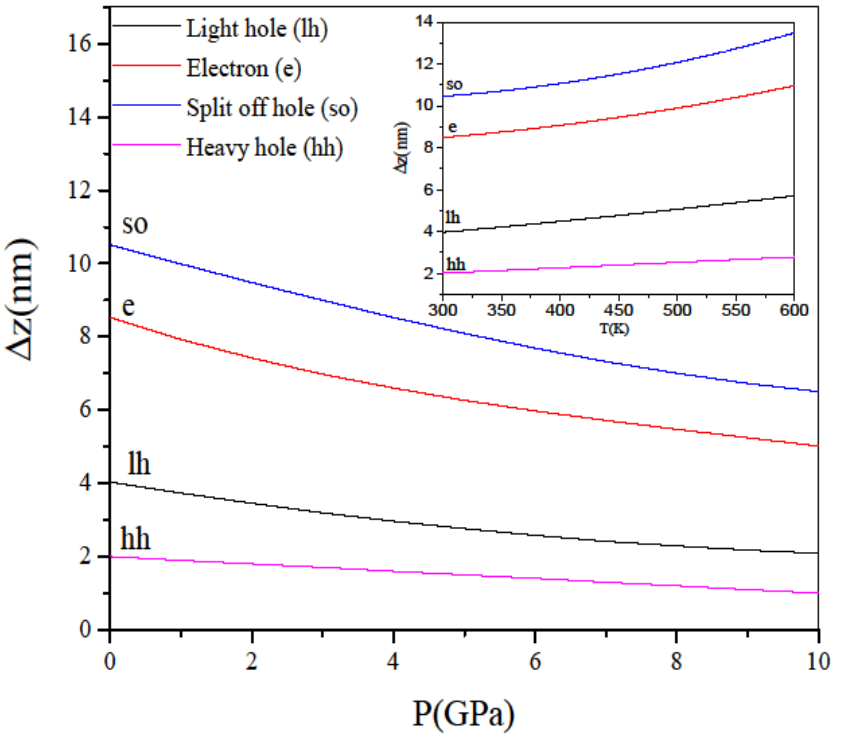

Fig. 8. Carrier localization length for the first subband of the heavy hole (hh), light hole (lh), electron (e), and split-off band hole (so) in InGaN/GaN MQW laser diodes under different hydrostatic pressures. The inset represents the variation of the localization length as a function of the temperature.

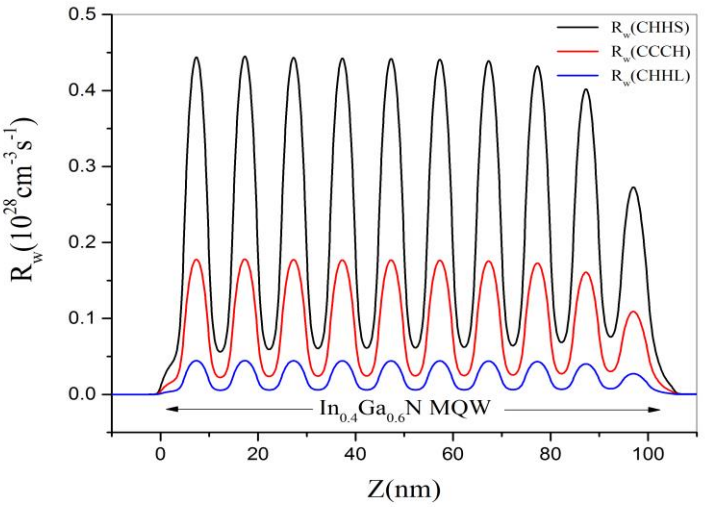

Fig. 9. Auger recombination rate of CHHS, CCCH, CHHL, and total InGaN wells in MQW laser diodes as a function of the distance.

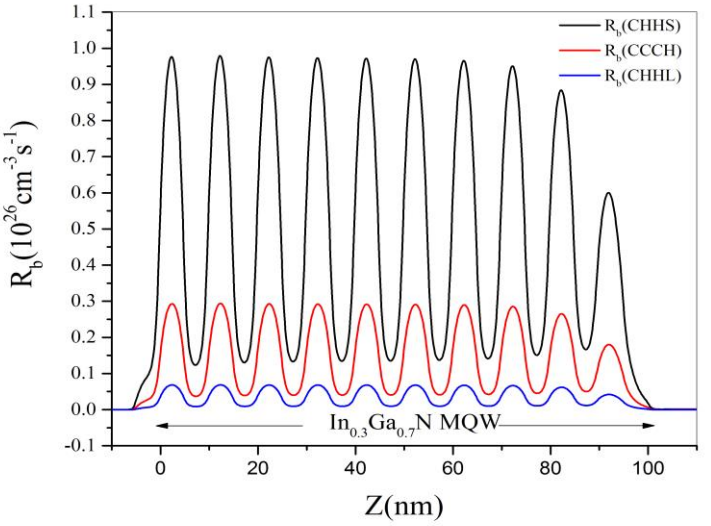

Fig. 10. Auger recombination rate of CHHS, CCCH, CHHL, and total InGaN barriers in MQW laser diodes regions as a function of the distance.

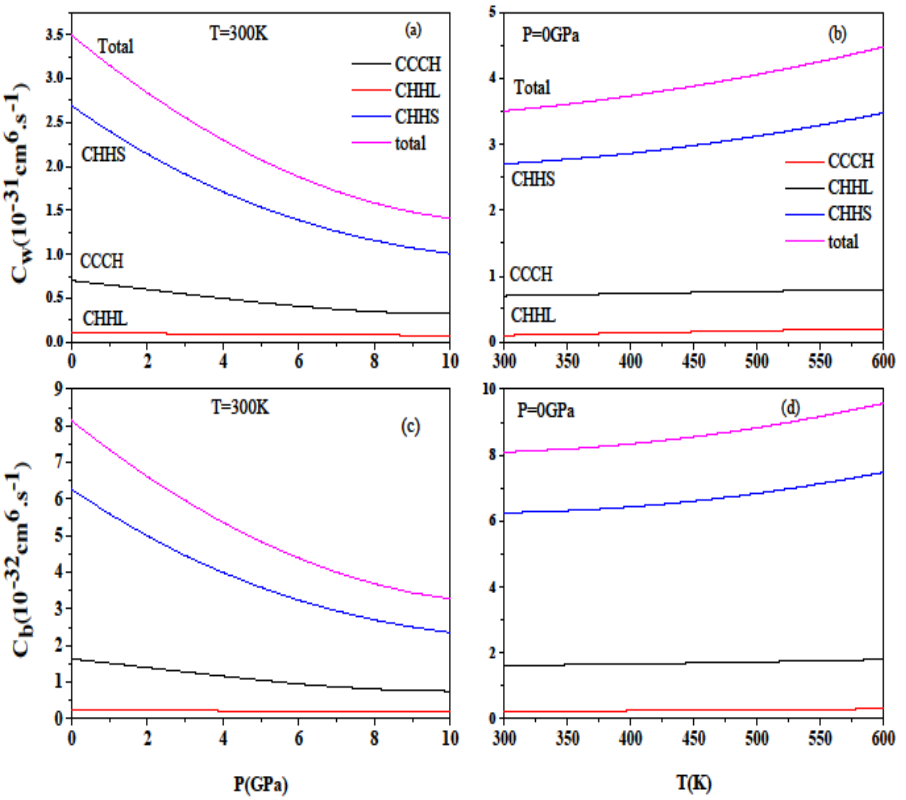

Fig. 11. Quantum well and barrier Auger coefficient of CHHS, CCCH, CHHL, and total InGaN/GaN MQW laser diodes as a function of hydrostatic pressure and temperature.

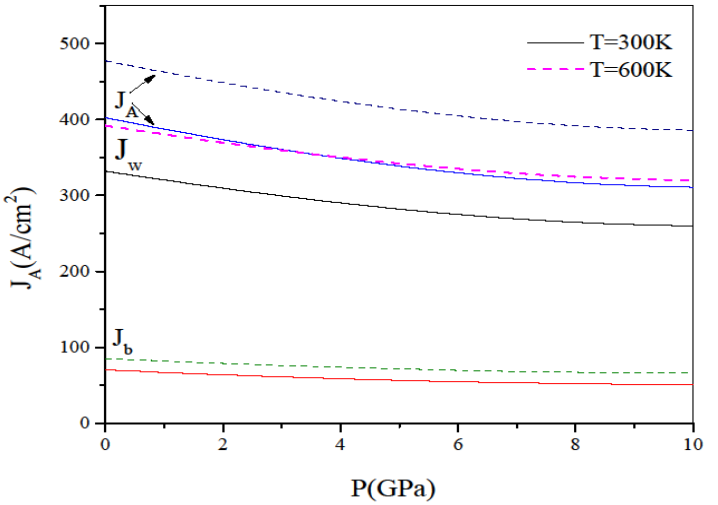

Fig. 12. Quantum well, barrier and total Auger current density of InGaN/GaN MQW laser diodes as a function of hydrostatic pressure and temperature.

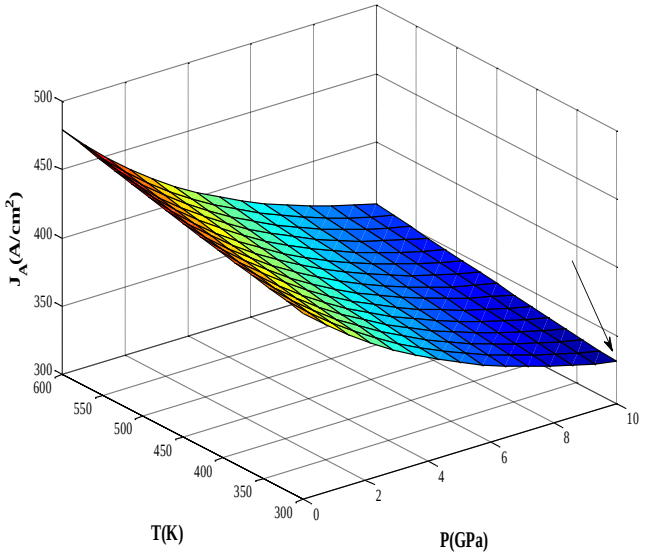

Fig. 13. Total Auger current density of InGaN/GaN MQW laser diodes as a function of hydrostatic pressure and temperature.

TABLE 1

Values of Auger coefficients resulting from experimental and numerical studies of InGaN/GaN MQW laser diodes at room temperature and P=0GPa.

Ref.	$C_w(10^{-31}cm^6s^{-1})$	$C_b(10^{-32}cm^6s^{-1})$	Description
This work	3.45	0.82	Numerical model
Bertazi et al.[48,49]	5	0.65	Numerical model
McMahon et al.[16]	3.3	-	Microscopic model
Kioupakis et al.[38]	-	0.9	First principles methodology
Piprek et al.[10]	2.5	-	APSYS* - Crosslight Software
Laubsch et al.[47]	3.5	-	Electroluminescence measurements and ABC model*

4. CONCLUSIONS

This study examined the optical and electrical parameters of c-plane InGaN/GaN MQWLDs under hydrostatic pressure and temperature. The results revealed that increasing the hydrostatic pressure could increase the amount of the carrier density and the electric field. On the other hand, this increase reduced the overlap integral of wave functions and the localized length of all carriers. Similarly, it decreased the Auger coefficient up to $2.1\times10^{-31}cm^6s^{-1}$ and $0.6\times10^{-31}cm^6s^{-1}$ in the multiple-quantum well and barrier regions, respectively, and decreased the total Auger current by $96A/cm^2$. However, with the increase in temperature in the range of 300-600K, all the electrical and optical parameters mentioned in the discussion of pressure are against the state of increasing pressure up to 10. In this case, the Auger coefficients and, consequently, the Auger current increase by $1.2\times10^{-31}cm^6s^{-1}$, $0.2\times10^{-31}cm^6s^{-1}$, and $73A/cm^2$, respectively. The performance of the laser diodes is better when the non-radiative Auger current is lower. Therefore, hydrostatic pressure plays a positive and temperature negative role in the performance of laser diodes. Also, for the hydrostatic pressure of about 10 GPa and the temperature of 300 K, the non-radiative Auger current has an optimum value of 334 A/cm^2.

Appendix A: Numerical Method

The discretization of Schrodinger and Poisson equations has been performed using finite difference method. A centered second order scheme is used. Therefore, a continuous term such as $\frac{d}{dz}\left(f\frac{d\psi}{dz}\right)$ is discretized according to:

$$\frac{d}{dz}\left(f\frac{d\psi}{dz}\right)=\frac{\frac{(f_{i+1}+f_i)}{2}\times\frac{(\psi_{i+1}-\psi_i)}{\Delta z}}{\Delta z} \tag{A1}$$

The Schrodinger equation becomes: $H\psi_i = E\psi_i$ The non-zero elements of the matrix H are:

$$H(i,j)=\begin{cases}\dfrac{\hbar^2}{2m_0\Delta z^2}\dfrac{1}{2}\left(\dfrac{1}{m^*(i)}+\dfrac{1}{m^*(i-1)}\right) & if \quad j=i+1\\ \dfrac{\hbar^2}{2m_0\Delta z^2}\left(\dfrac{1}{2}\left(\dfrac{1}{m^*(i)}+\dfrac{1}{m^*(i-1)}\right)+\dfrac{1}{2}\left(\dfrac{1}{m^*(i)}+\dfrac{1}{m^*(i+1)}\right)\right)+E_C(i) & j=i\\ -\dfrac{\hbar^2}{2m_0\Delta z^2}\dfrac{1}{2}\left(\dfrac{1}{m^*(i)}+\dfrac{1}{m^*(i+1)}\right) & j=i+1\end{cases} \tag{A2}$$

The above eigenvalues system and linear system are coupled and should be solved using an iterative method. The convergence is obtained when the difference on the Fermi level associated to two consecutive iterations is smaller than $10^{-4}eV$. The boundary conditions related to Schrodinger equation are:

$$\psi_n(z=0)=\psi_n(z=L)=0 \tag{A3}$$

where L is the total height of the structure. The boundary conditions related to Poisson equation are:

$$\left.\frac{d(V_H+V_P)}{dz}\right|_{z=0}=\left.\frac{d(V_H+V_P)}{dz}\right|_{z=L}=0 \tag{A4}$$

The details of the self-consistent solution of the Schrodinger-Poisson equation are as follows:

1- Consider the optional value for n_{2D} .

2- Solve the Poisson equation.

3- Solve the Schrodinger equation and obtain the wave functions and their energy sub-bands.

4- Using the following equations, we obtain the electron density and the Fermi energy [17, 39].

$$E_F = E_0 + (\pi\hbar^2 n_{2D})/m^* \quad \text{(A5)}$$

$$E_0 = (9\pi\hbar^2 e^2 n_{2D})/(8\varepsilon_0\sqrt{8m^*}\,\varepsilon_{GaN}) \quad \text{(A6)}$$

5- If it is $E_{F(n)} - E_{F(n-1)} < 10^{-4} eV$, the self-consistent program will end. Otherwise($E_{F(n)} - E_{F(n-1)} > 10^{-4} eV$), put new n_{2D} in Schrodinger's equation and continue the program until condition $E_{F(n)} - E_{F(n-1)} < 10^{-4} eV$ is established.

For mesh refinement in the numerical calculation written in the Matlab software, commands initmesh and refinemesh are performed as follows in different regions of structure InGaN/GaN.

fem. mesh= initmesh (fem,'hmax',[.05e-9],'hmaxfact',1,'hgrad',1.3, 'zscale',1.0);
fem. mesh= refinemesh (fem, 'mcase',0);

Where there are fem commands in solving wave functions, hmax is the maximum edge size which is equal to 0.05e-9m, hgrad is the mesh growth rate which is equal to 1.3, zscale is a region to be refined.

REFRENCES

[1] A. David, N. G. Young, C. Lund, M. D. Craven. *Compensation between radiative and Auger recombinations in III-nitrides: The scaling law of separated-wavefunction recombinations*. Appl. Phys. Lett. 115 (2019) 193502.Available:https://iopscience.iop.org/article/10.1149/2.0372001JSS

[2] C.K. Tan, W. Sun, J. J. WiererJr. N. Tansu. *Effect of interface roughness on Auger recombination in semiconductor quantum wells*. AIP Advances. 7, 035212 (2017). Available: https://pubs.aip.org/aip/adv/article/7/3/035212/1023080

[3] D. Steiauf, E. Kioupakis, C. G. Van de Walle. Auger Recombination in GaAs from First Principles, ACS Photonics. 1 (2014) 643. Available: https://pubs.acs.org/doi/abs/10.1021/ph500119q

[4] D.P. Han, C.H. Oh, D.G. Zheng, H. Kim, J.I. Shim, K. S. Kim, D. S. Shin. *Analysis of nonradiative recombination mechanisms and their impacts on the device performance of InGaN/GaN light-emitting diodes*. Jpn. J. Appl. Phys.54 (2015) 02BA01. Available: https://iopscience.iop.org/article/10.7567/JJAP.54.02BA01

[5] W. Liu, C. Haller, Y. Chen, T. Weatherly, J.-F. Carlin, G. Jacopin, R. Butté, N. Grandjean. *Impact of defects on Auger recombination in c-plane InGaN/GaN single quantum well in the efficiency droop regime*. Appl. Phys. Lett. 116 (2020) 222106. Available: https://pubs.aip.org/aip/apl/article/116/22/222106/38539

[6] E. Kioupakis, P. Rinke, K. T. Delaney, C. G. Van de Walle. *Indirect Auger recombination as a cause of efficiency droop in nitride light-emitting diodes*. Appl. Phys. Lett, 98, (2011) 161107**.** Available: https://pubs.aip.org/aip/apl/article-abstract/98/16/161107/340399

[7] J. Piprek. *Efficiency droop in nitride-based light-emitting diodes*. Phys. Status Solidi A. 207(10) (2010) 2217–2225. Available: https://onlinelibrary.wiley.com/doi/10.1002/pssa.201026149

[8] M. Auf der Maur, G. Moses, J. M. Gordon, X. Huang, Y. Zhao, E. A. Katz. *Temperature and intensity dependence of the open-circuit voltage of InGaN/GaN multi-quantum well solar cells*. Sol. Energy Mater Sol. Cells. 230 (2021) 111253. Available: https://www.sciencedirect.com/science/article/pii/S092702482100297X

[9] Y. Sefidgar, H. R. Saghai, H. G. K. Azar. *Enhancing Efficiency of Twobond Solar Cells Based on GaAs/InGaP*. Journal of Optoelectronical Nanostructures. 4(2) (2019) 84-102. Available: https://jopn.marvdasht.iau.ir/article_3480_0b715e5dbfb8c90033530e34eb33a84a.pdf

[10] J. Piprek, F. Römer, B. Witzigmann. *On the uncertainty of the Auger recombination coefficient extracted from InGaN/GaN light-emitting diode efficiency droop measurements*. Appl. Phys. Lett. 106 (2015) 101101. Available: https://www.nusod.org/piprek/piprek15apl.pdf

[11] H.-Y. Ryu, G.H. Ryu, C. Onwukaeme. *B. Ma, Temperature dependence of the Auger recombination coefficient in InGaN/GaN multiple-quantum-*

well light-emitting diodes. Opt. Express. 28(19) (2020) 27459. Available: https://pubmed.ncbi.nlm.nih.gov/32988039

[12] L. Cheng, Z. Li, J. Zhang, X. Lin, D. Yang, H. Chen, S. Wu, S. Yao. *Advantages of InGaN–GaN–InGaN Delta Barriers for InGaN-Based Laser Diodes.* Nanomaterials. 11 (2021) 2070. Available: https://www.mdpi.com/2079-4991/11/8/2070

[13] S. Picozzi, R. Asahi, C. B. Geller, A. J. Freeman. *Accurate First-Principles Detailed-Balance Determination of Auger Recombination and Impact Ionization Rates in Semiconductors*. Phys. Rev. Lett. 89(19) (2002) 197601. Available: https://journals.aps.org/prl/abstract/10.1103/PhysRevLett.89.197601

[14] A. S. Polkovnikov, G. G. Zegrya. *Auger recombination in semiconductor quantum wells*. Phys. Rev. B, 58(7) (1998) 4039-4056. Available: https://journals.aps.org/prb/abstract/10.1103/PhysRevB.58.4039

[15] J. Piprek. *Efficiency Models for GaN-Based Light-Emitting Diodes: Status and Challenges*. Materials, 13 (2020) 5174. Available: https://www.mdpi.com/1996-1944/13/22/5174

[16] J. M. McMahon, E. Kioupakis, S. Schulz. *Atomistic analysis of Auger recombination in c-plane (In,Ga)N/GaN quantum wells: Temperature-dependent competition between radiative and nonradiative recombination*. Phys. Rev. B. 105 (2022) 195307. Available: https://journals.aps.org/prb/abstract/10.1103/PhysRevB.105.195307

[17] H. Belmabrouk,, B. Chouchen , E. M. Feddi , F. Dujardin , I. Tlili , M. B. Ayed, M.Hichem Gazzah. *Modeling the simultaneous effects of thermal and polarization in InGaN/GaN based high electron mobility transistors*. Optik, 207 (2020) 163883. Available: https://www.sciencedirect.com/science/article/pii/S0030402619317814

[18] X Huang et al. *Piezo-Phototronic Effect in a Quantum Well Structure*. ACS Nano. 10(5) (2016) 5145. Available: https://pubs.acs.org/doi/10.1021/acsnano.6b00417

[19] B. K. Ridley, W. J. Schaff, and L. F. Eastman. *Theoretical model for polarization superlattices: Energy levels and intersubband transitions*. J. Appl. Phys. 94 (2003) 3972. Available: https://pubs.aip.org/aip/jap/article-abstract/94/6/3972/292303

[20] O. Ambacher, J. Majewski, C. Miskys, et al. *Pyroelectric properties of Al(In)GaN/GaN hetero- and quantum well structures* J. Phys. Condens. Matter. 14 (2002) 3399. Available: https://iopscience.iop.org/article/10.1088/0953-8984/14/13/302

[21] A. Asgari, K. Khalili. *Temperature dependence of InGaN/GaN multiple quantum well based high efficiency solar cell*. Sol. Energy Mater Sol. Cells. 95 (2011) 3124–3129. Available: https://www.sciencedirect.com/science/article/pii/S0927024811003898

[22] V. Fiorentini. *Evidence for nonlinear macroscopic polarization in III–V nitride alloy heterostructures*. Appl. Phys. Lett. 80 (2002) 1204. Available: https://pubs.aip.org/aip/apl/article-abstract/80/7/1204/511321

[23] P. Perlin, L. Mattos, N. A. Shapiro, J. Kruger, W. S. Wong, T. Sands. *Reduction of the energy gap pressure coefficient of GaN due to the constraining presence of the sapphire substrate*. J. Appl. Phys. 85 (1999) 2385. Available: https://pubs.aip.org/aip/jap/article-abstract/85/4/2385/491363

[24] K. J. Bala, A. J. Peter, C. W. Lee. *Simultaneous effects of pressure and temperature on the optical transition energies in a* $Ga_{0.7}In_{0.3}N/GaN$ *quantum ring*. Chem. Phys. 495 (2017) 42–47. Available: https://www.sciencedirect.com/science/article/pii/S0301010417304160

[25] S. L. Chuang, C. S. Chang. *A band-structure model of strained quantum-well wurtzite semiconductors*. Semicond. Sci. Technol. 12 (1997) 252–263. Available:

[26] S. L. Chuang and C. S. Chang. *k.p method for strained wurtzite semiconductors*. Phys. Rev. B. 54(4) (1996) 2491-2504. Available: https://journals.aps.org/prb/abstract/10.1103/PhysRevB.54.2491

[27] J. Piprek and S. Nakamura. *Physics of high-power InGaN/GaN lasers*. IEE Proceedings – Optoelectronics. 149(4) (2002) 145–151. Available: https://www.nusod.org/piprek/piprek02iee.pdf

[28] A. Venkatachalam, P.D. Yoder, B. Klein, A. Kulkarni, Nitrid band-structure model in quantum well laser simulater. Opt Quant Electron. 40 (2008) 295. https://link.springer.com/article/10.1007/s11082-008-9199-4

[29] A. D. Andrew, E. O. O'Reilly. *Theoretical study of Auger recombination in a GaInNAs 1.3 μm quantum well laser structure*. Appl. Phys. Lett. 84 (2004) 182. Available: https://pubs.aip.org/aip/apl/article-abstract/84/11/1826/531040

[30] J. Wang, P. V. Allmen, J.-P. Leburton, K. J. Linden. *Auger Recombination in Long- Wavelength Strained-Layer Quantum-Well Structures*. IEEE J. Quantum Electron**.** 31(5) (1995) 864-875. Available: https://ieeexplore.ieee.org/document/375931

[31] A. Asgari, M. Kalafi, L. Faraone. *A quasi-two-dimensional charge transport model of AlGaN/GaN high electron mobility transistors (HEMTs)*. Physica E. 28 (2005) 491–499. Available: https://www.sciencedirect.com/science/article/pii/S1386947705002183

[32] D. Watson-Parris, M. J. Godfrey, P. Dawson. *Carrier localization mechanisms in $In_xGa_{1-x}N$/GaN quantum wells*. Phys. Rev. B. 83 (2011) 115321. Available: https://journals.aps.org/prb/abstract/10.1103/PhysRevB.83.115321

[33] R. Yahyazadeh. *Effect of hydrostatic pressure on the radiative current density of InGaN/GaN multiple quantum well light emitting diodes*. Opt Quant Electron. 53 (2021) 571. Available: https://link.springer.com/article/10.1007/s11082-021-03236-9

[34] R Yahyazadeh, Z Hashempour. *Numerical Modeling of Electronic and Electrical Characteristics of Al Ga N / GaN Multiple Quantum Well Solar Cells*, J. Optoelectron. Nanostruct. 5(3) (2020) 81. Available: https://jopn.marvdasht.iau.ir/article_4406_670911b9469aba0ae5aa327d5bb3b34e.pdf

[35] R. Yahyazadeh. *Effect of hydrostatic pressure on the photocurrent density of InGaN/GaN multiple quantum well solar cells*. Indian Journal of Physics. 96 (2022) 2815. Available: https://link.springer.com/article/10.1007/s12648-021-02218-7

[36] R. Yahyazadeh. *Numerical modeling of electronic and electrical characteristics of InGaN/GaN multiple quantum well solar cells*. Journal of Photonics for Energy. 10 (2020) 045504. Available: https://www.spiedigitallibrary.org/journals/journal-of-photonics-for energy//10.1117/1.JPE.10.045504

[37] R. yahyazadeh, Z. Hashempour. *Effect of Hydrostatic Pressure on Optical Absorption Coefficient of InGaN/GaN of Multiple Quantum Well Solar Cells*. Journal of Optoelectronical Nanostructures. 6(2) (2021) 1. Available: https://jopn.marvdasht.iau.ir/article_4768_17586fedc153930972ae0f3cb2317226.pdf

[38] E. Kioupakis, D. Steiauf, P. Rinke, K.ris T. Delaney, C. G. Van de Walle. *First-principles calculations of indirect Auger recombination in nitride semiconductors*. Phys. Rev. B. 92 (2015) 035207. Available: https://journals.aps.org/prb/abstract/10.1103/PhysRevB.92.035207

[39] B. Chouchen, M. H. Gazzah, A. Bajahzar, H. Belmabrouk. *Numerical modeling of InGaN/GaN p-i-n solar cells under temperature and hydrostatic pressure effects*. AIP Adv. 9 (2019) 045313. Available: https://pubs.aip.org/aip/adv/article/9/4/045313/1076706

[40] B. Jogai. *Influence of surface states on the two-dimensional electron gas in AlGaN/GaN heterojunction field-effect transistors*. J. Appl. Phys. 93 (2003) 1631. Available: https://pubs.aip.org/aip/jap/article-abstract/93/3/1631/293059

[41] B. Jogai. *Parasitic Hole Channels in AlGaN/GaN Heterojunction Structures*. Phys. stat. sol (b). 233 (2002) 506. Available:https://onlinelibrary.wiley.com/doi/epdf/10.1002/1521-3951(200210)233:3<506::aid-pssb506>3.0.co;2-r

[42] A. Horri, S. Z. Mirmoeini. *Analysis of Kirk Effect in Nanoscale Quantum Well Heterojunction Bipolar Transistor Laser*. Journal of Optoelectronical Nanostructures. 5(2) (2020) 25-38. Available: https://jopn.marvdasht.iau.ir/article_4216_16b679cf6224faf5b5bb84a468ea2283.pdf

[43] M. Amirhoseiny, G. Alahyarizadeh. *Enhancement of Deep Violet InGaN Double Quantum WellsLaser Diodes Performance Characteristics Using Superlattice Last Quantum Barrier*. Journal of Optoelectronical Nanostructures. 6(2) (2021) 107-120. Available: https://jopn.marvdasht.iau.ir/article_4776_4941a2547e09c61dfc979b5fed25a722.pdf

[44] V. B. Yekta, H. Kaatuzian. *Design considerations to improve high temperature characteristics of 1.3 μm AlGaInAs-InP uncooled multiple quantum well lasers: Strain in barriers*. Optik. 122 (2011) 514. Available:https://www.sciencedirect.com/science/article/pii/S0030402610001567

[45] J. Hader; J.V. Moloney, S.W. Koch. *Microscopic evaluation of spontaneous emission- and Auger-processes in semiconductor lasers*. IEEE J. Quantum Electron. 41(10) (2005) 1217- 1226. Available: https://ieeexplore.ieee.org/document/1510789

[46] I.H. Tan, G. L. Snider, L. D. Chang, E. L. Hu. *A self-consistent solution of Schrödinger–Poisson equations using a nonuniform mesh*. J. Appl. Phys. 68 (1990) 4071. Available: https://pubs.aip.org/aip/jap/article-abstract/68/8/4071/19325

[47] A. Laubsch, M. Sabathil, J. Baur, M. Peter, B. Hahn. *High-Power and High-Efficiency InGaN-Based Light Emitters*. EEE Trans Electron Devices. 57(1) (2010) 79 – 87. Available: https://ieeexplore.ieee.org/document/5345808

[48] F. Bertazzi, X. Zhou, M. Goano, G. Ghione, E. Bellotti. *Auger recombination in InGaN/GaN quantum wells: A full-Brillouin-zone study*. Appl. Phys. Lett. 103 (2013) 081106. Available: https://pubs.aip.org/aip/apl/article-abstract/103/8/081106/130246

[49] F. Bertazzi, M. Goano, E. Bellotti. *A numerical study of Auger recombination in bulk InGaN*. Appl. Phys. Lett. 97 (2010) 231118. Available: https://pubs.aip.org/aip/apl/article abstract/97/23/231118/325187